Supporting Information

Dinuclear Mono-bridged or Polymeric Lanthanide Complexes from One Ligand: Structural Transformation and Chiral Induction

Ran Chen,[a, b] Qian-Qian Yan, [a, b] Shao-Jun Hu,[a] Xiao-Qing Guo,[a] Li-Peng Zhou, [*a] and Qing-Fu Sun[*a, b]

a. State Key Laboratory of Structural Chemistry, Fujian Institute of Research on the Structure of Matter, Chinese Academy of Sciences, Fuzhou 350002, People's Republic of China.

b. College of Chemistry, Fuzhou University, Fuzhou 350108, People's Republic of China.

Table of contents

1. General

Unless otherwise stated, all chemicals and solvents were purchased from commercial companies and used without further purification. Deuterated solvents were purchased from Admas, J&K scientific and Sigma-Aldrich. 1D and 2D NMR were measured on a Bruker Biospin Avance III (400 MHz) spectrometer or JNM-ECZ600R/S1 (600 MHz) spectrometer. ^{1}H-NMR chemical shifts were determined with tetramethylsilane (TMS) or respected to residual signals of the deuterated solvents used. ESI-TOF-MS were recorded on an Impact II UHR-TOF mass spectrometry from Bruker, with tuning mix as the internal standard. Data analysis was conducted with the Bruker Data Analysis software (Version 4.3) and simulations were performed with the Bruker Isotope Pattern software. X-ray crystallography analysis of single crystal was performed on a Bruker D8 VENTURE photon II diffractometer with Iμs 3.0 microfocus X-ray source diffractometer. Data reduction was performed with the APEX-III software. Structures were solved by direct methods and refined by full-matrix least-squares on F2 with anisotropic displacement using the SHELX software package. Solvent molecules were highly disordered and could not be reasonably located. These residual intensities were removed by PLATON/SQUEEZE routine. Crystal data and final refinement details for the structures are reported in Table S1 and S2. CD spectra were recorded on a MOS-450 circular dichroism spectrometer.

2. Experimental procedures

Scheme S1. Synthetic routes of organic ligands **L** and the self-assemblies.

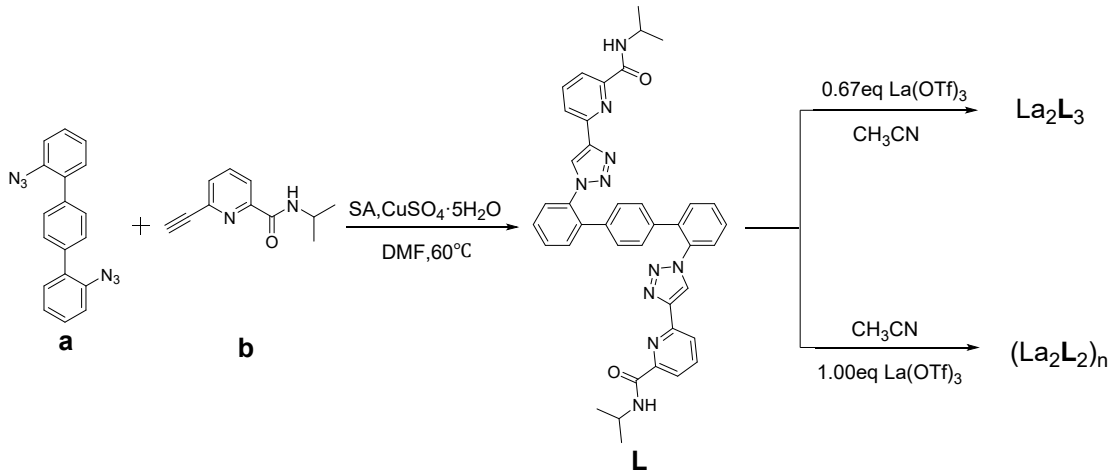

Compounds **a** and **b** were prepared acccording to the reference procedure.[1, 2]

Synthesis of L： Compound **a** (231.1mg, 0.74mmol, 1.0 equiv)**, b** (284.2 mg, 1.51 mmol, 2.5 equiv) were added into the DMF solution (30 ml) containing sodium

ascorbate (206.2 mg, 1.04 mmol, 1.4 equiv) and $CuSO_4 \cdot 5H_2O$ (110 mg, 0.45mmol, 0.6 equiv) and the mixture was stirred at 60 °C for 24 h. After filtration, the solvent was removed under reduced pressure and the crude product was purified chromatographically (SiO_2, DCM/PE = 2:1) to afford **L** as white solid (364.9 mg，71.6％ yield). ^{1}H NMR (400 MHz, $CDCl_3$, 298 K) δ 8.19 (d, *J* = 7.8 Hz, 1H), 8.13 (d, *J* = 7.7 Hz, 1H), 7.95 – 7.88 (m, 2H), 7.67 (d, *J* = 8.2 Hz, 1H), 7.63 – 7.51 (m, 3H), 7.48 (d, *J* = 7.7 Hz, 1H), 7.12 (s, 2H), 4.21 (m, 1H), 1.19 (d, *J* = 6.6 Hz, 6H). ^{13}C NMR (101 MHz, $CDCl_3$, 298 K) δ 163.11, 149.90, 148.43, 147.39, 138.30, 137.08, 136.69, 134.77, 131.30, 130.41, 128.88, 128.81, 126.68, 124.13, 122.78, 121.52, 41.38, 22.69. Elemental analysis: Calcd for $C_{40}H_{36}N_{10}O_2 \cdot H_2O$: C, 67.97 %; H, 5.42 %; N, 19.82 %. Found: C, 67.28 %; H, 5.24 %; N, 19.27 %. ESI-TOF-MS: $C_{40}H_{36}N_{10}O_2$ $[M+Na]^+$, calculated: m/z = 711.2915; observed: m/z = 711.2879.

Synthesis of $La_2\mathbf{L}_3$**：** 1.00 eq **L** (3.8 mg, 5.5 μmol) was treated with 0.67 eq $La(OTf)_3$ (2.2 mg, 3.7 μmol) in CD_3CN (600 μl) at 50 °C and stirred for 10 minutes, a homogeneous faint yellow solution was obtained. Elemental analysis: Calcd for $La_2(C_{40}H_{36}N_{10}O_2)_3(CF_3SO_3)_6 \cdot 6H_2O$: C, 45.22 %; H, 3.61 %; N, 12.56 %. Found: C, 45.05 %; H, 3.77 %; N, 12.58 %. ESI-TOF-MS for $[(La_2\mathbf{L}^{\boldsymbol{R}}_3)(OTf)_4]^{2+}$ calcd, m/z: 1469.7647; found: 1469.7644.

Synthesis of $(La_2\mathbf{L}_2)_n$**：** 1.00 eq **L** (3.8 mg, 5.5 μmol) was treated with 1.00 eq $La(OTf)_3$ (3.2 mg, 5.5 μmol) in CD_3CN (600 μl) at 50 °C and stirred for 10 minutes, a homogeneous faint yellow solution was obtained. ^{1}H NMR (600MHz, CD_3CN, 298K) δ 8.74 (s, 1H), 8.32 (d, *J* = 7.7 Hz, 1H), 8.25 (t, 8.0 Hz, 1H), 8.07 (d, *J* = 8.0 Hz, 2H), 7.73 (m, 1H), 7.66 (m, 3H), 7.16 (d, *J* = 8.4 Hz, 1 H), 6.94 (d, *J* = 8.4 Hz, 1 H), 4.15 (m, 1H), 1.27 (d, *J* = 6.6 Hz, 3H), 1.17 (d, *J* = 6.6 Hz, 3H). Elemental analysis: Calcd for $[La_2(C_{40}H_{36}N_{10}O_2)_2(CF_3SO_3)_6 \cdot 6H_2O]_n$: C, 38.86 %; H, 3.19 %; N, 10.54 %. Found: C, 38.50 %; H, 3.38 %; N, 10.54 %.

Synthesis of *Δ*-La$\mathbf{LG}^{\boldsymbol{R}}$**：** 1.00 eq **L** (3.8 mg, 5.5 μmol) and 1.00 eq $\mathbf{G}^{\boldsymbol{R}}$ (2.0 mg, 5.5 μmol) was treated with 1.00 eq $La(OTf)_3$ (3.2 mg, 5.5 μmol) in CD_3CN (600 μl) at 50 °C and stirred for 10 minutes, a homogeneous faint yellow solution was obtained. ^{1}H NMR (400 MHz, CD_3CN) δ 8.93 (s, 1H), 8.78 (d, *J* = 7.0 Hz, 1H), 8.65 (s, 1H), 8.55 (t, *J* = 8.0 Hz, 1H), 8.39 (d, *J* = 7.8 Hz, 1H), 8.21 (d, *J* = 7.1 Hz, 1H), 8.03 (t, *J* = 7.6 Hz, 1H), 7.99 (t, *J* = 7.8 Hz, 1H), 7.85-7.69 (m, 6H), 7.67-7.55 (m, 6H), 7.46 (t, *J* = 7.6 Hz, 2H), 7.38 (d, *J* = 7.4 Hz, 1H), 7.27 (d, *J* = 7.8 Hz, 1H), 7.05-6.88 (m, 9H), 6.72 (d, *J* = 7.4 Hz, 2H), 6.61 (d, *J* = 7.4 Hz, 2H), 5.32 (dd, *J* = 10.3, 7.3 Hz, 1H), 5.08 (t, *J* = 9.8 Hz, 1H), 4.77 (t, *J* = 9.8 Hz, 1H), 4.50 (dd, *J* = 10.1, 6.8 Hz, 1H), 4.31 – 4.24 (m, 1H), 4.21 (dd, *J* = 9.2, 6.8 Hz, 1H), 4.03 (m, 1H), 3.72 (m, 1H), 1.33 (d, *J* = 6.6 Hz, 3H), 1.19 (d, *J* = 6.7 Hz, 3H), 1.12 (d, *J* = 6.6 Hz, 3H), 0.65 (d, *J* = 6.5 Hz, 3H). Elemental analysis: Calcd for $La(C_{40}H_{36}N_{10}O_2)(C_{23}H_{19}N_3O_2)(CF_3SO_3)_3 \cdot 2H_2O$: C, 47.18 %; H, 3.54 %; N, 10.84 %. Found: C, 47.05 %; H, 3.67 %; N, 10.87 %. ESI-TOF-MS for $[La\mathbf{LG}^{\boldsymbol{R}}(OTf)_1]^{2+}$: calcd. 672.6536, found 672.6531; for $[La\mathbf{LG}^{\boldsymbol{R}}(OTf)_2]^{+}$: calcd. 1494.2599, found 1494.2594.

Δ-La**LG**^{R} could be also obtained by adding equimolar auxiliary ligand **G**^{R} relative to the lanthanum ion into the CD_3CN solution of $La_2\mathbf{L}_3$ or $(La_2\mathbf{L}_2)_n$.

Δ-La**LG**^{S} was prepared by **G**^{S} in a similar procedure. Elemental analysis: Calcd for $La(C_{40}H_{36}N_{10}O_2)(C_{23}H_{19}N_3O_2)(CF_3SO_3)_3\cdot 2H_2O$: C, 47.18 %; H, 3.54 %; N, 10.84 %. Found: C, 47.09 %; H, 3.68 %; N, 10.86 %. ESI-TOF-MS for $[La\mathbf{LG}^{S}(OTf)_1]^{2+}$: calcd. 672.6536, found 672.6530; for $[La\mathbf{LG}^{R}(OTf)_2]^{+}$: calcd. 1494.2599, found 1494.2589.

3. NMR spectra

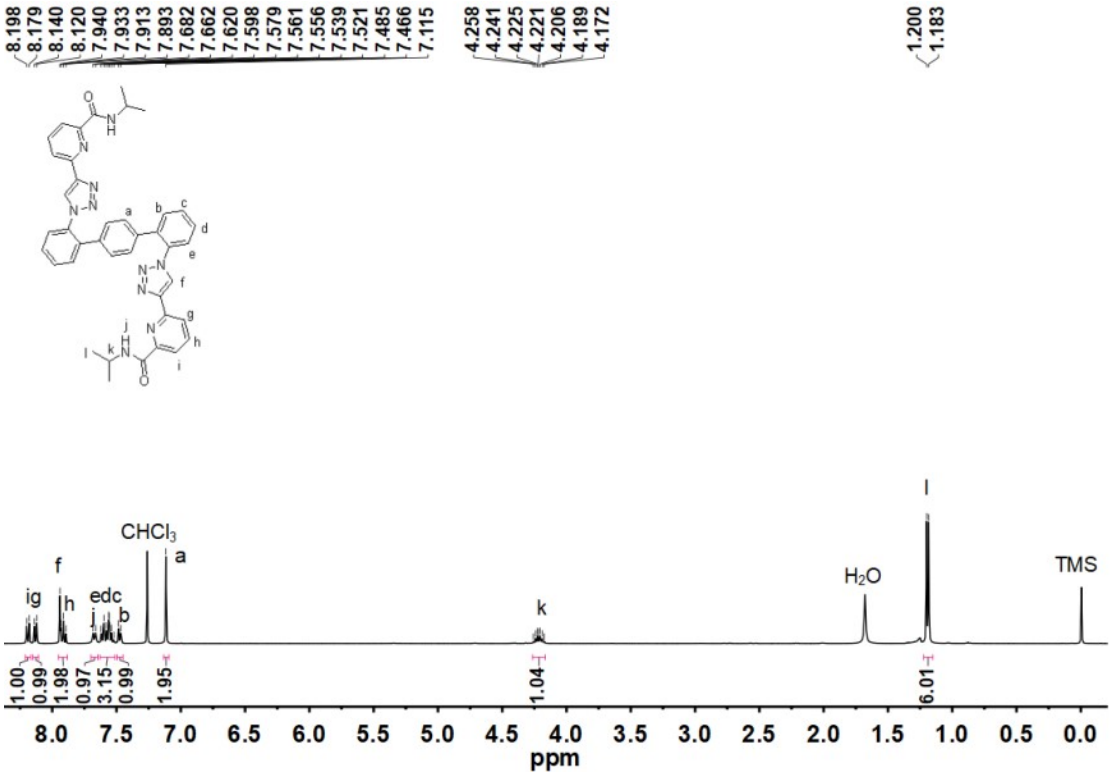

Fig. S1 ^{1}H NMR spectrum of **L** (400 MHz, $CDCl_3$, 298K).

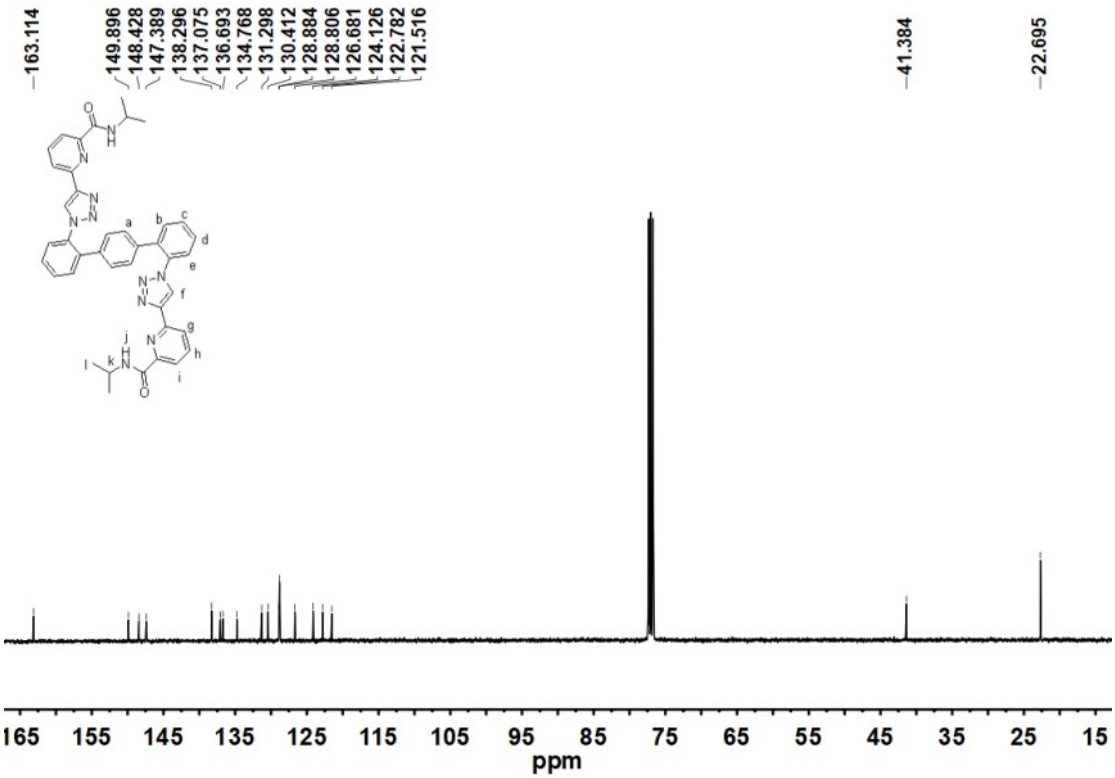

Fig. S2 ^{13}C NMR spectrum of **L** (101 MHz, $CDCl_3$, 298K).

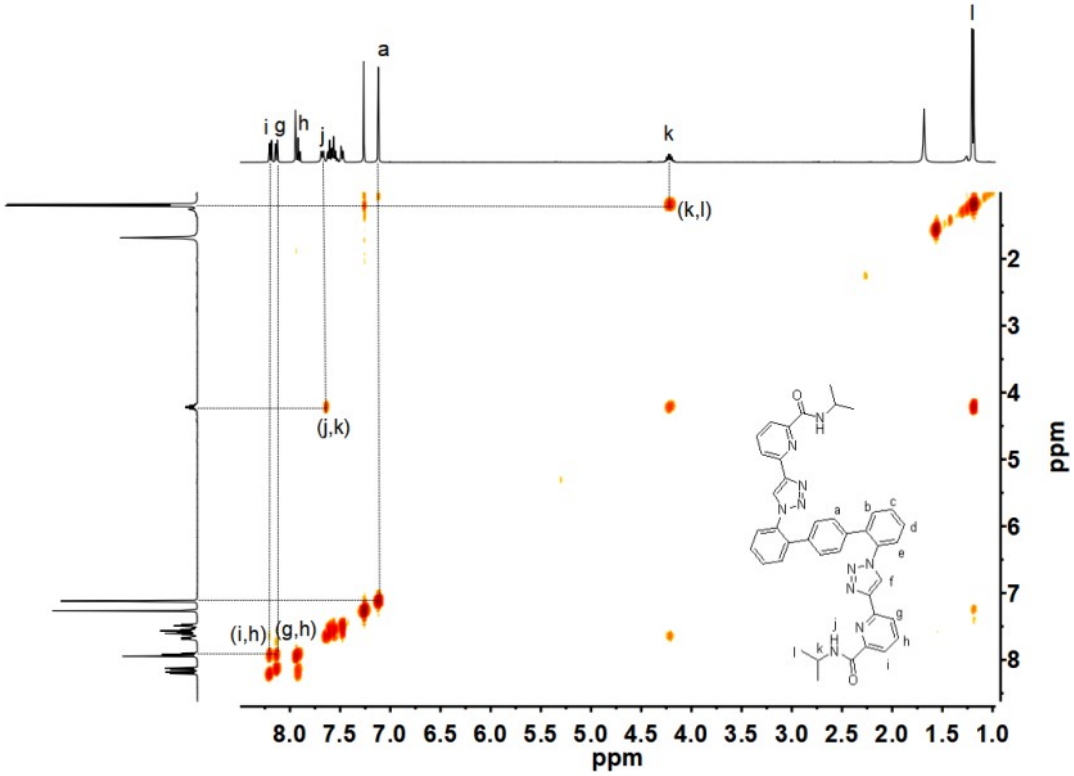

Fig. S3 ^{1}H-^{1}H COSY NMR spectrum of **L** (400 MHz, $CDCl_3$, 298 K).

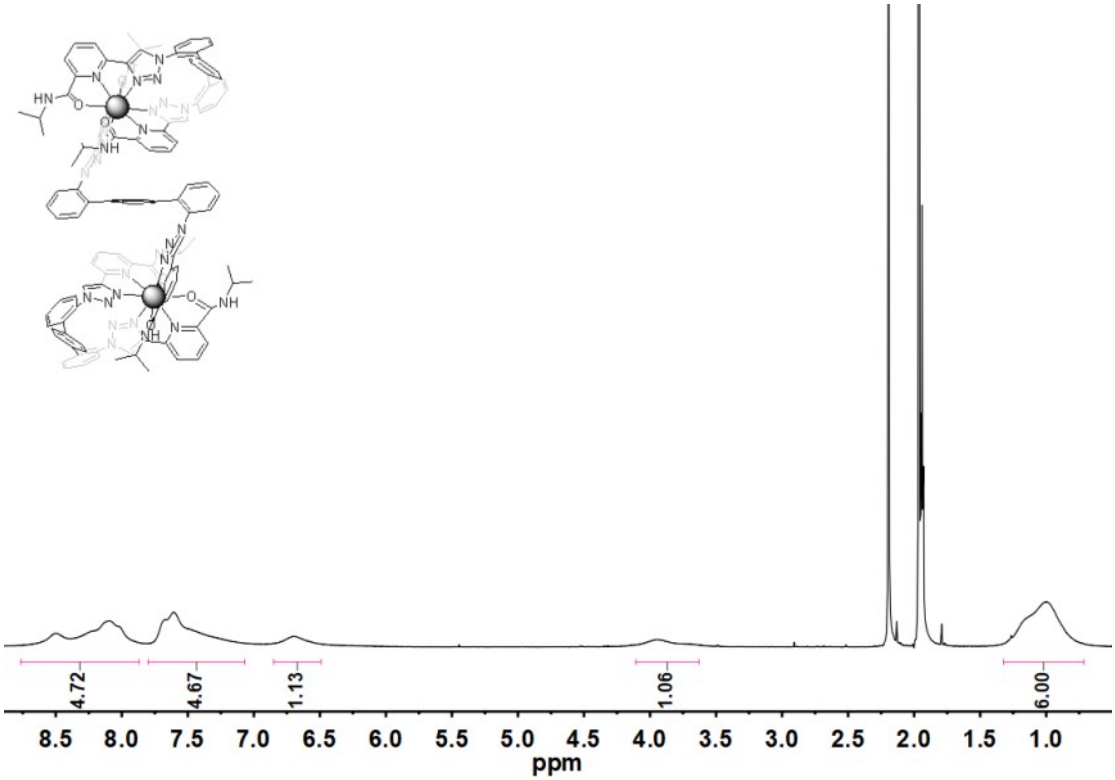

Fig. S4 ^{1}H NMR spectrum of $La_2\mathbf{L}_3$ (400MHz, CD_3CN, 298K).

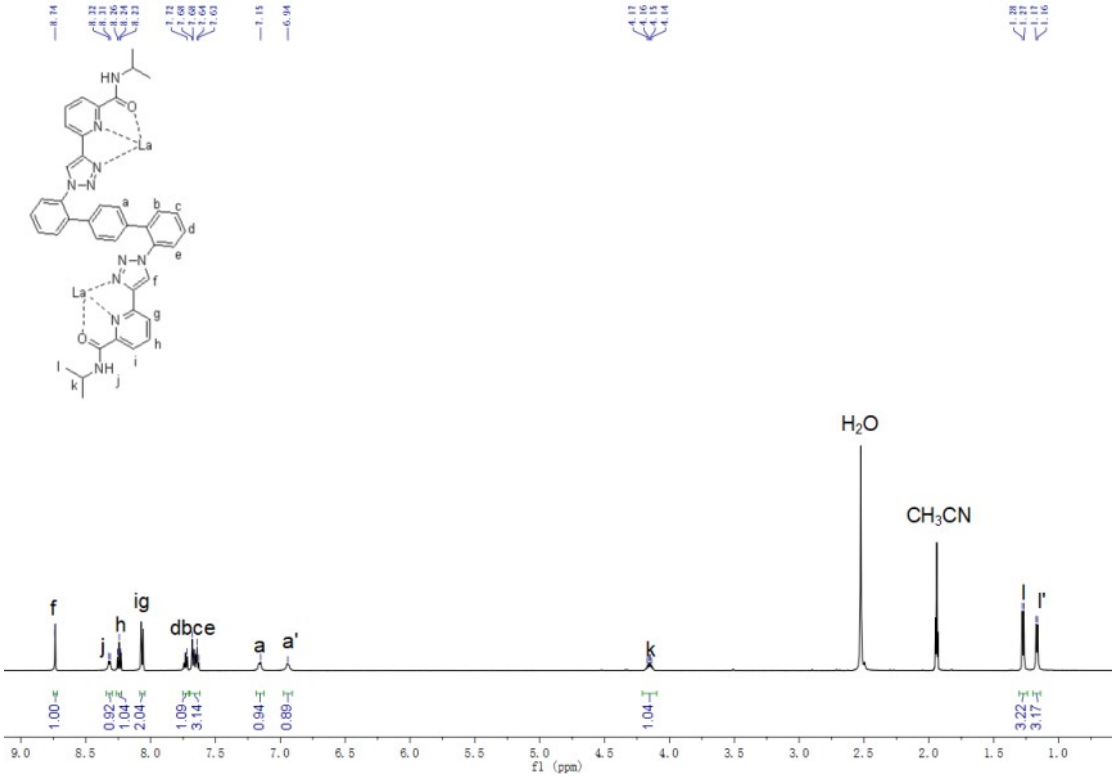

Fig. S5 ^{1}H NMR spectrum of $(La_2\mathbf{L}_2)_n$ (600MHz, CD_3CN, 298K).

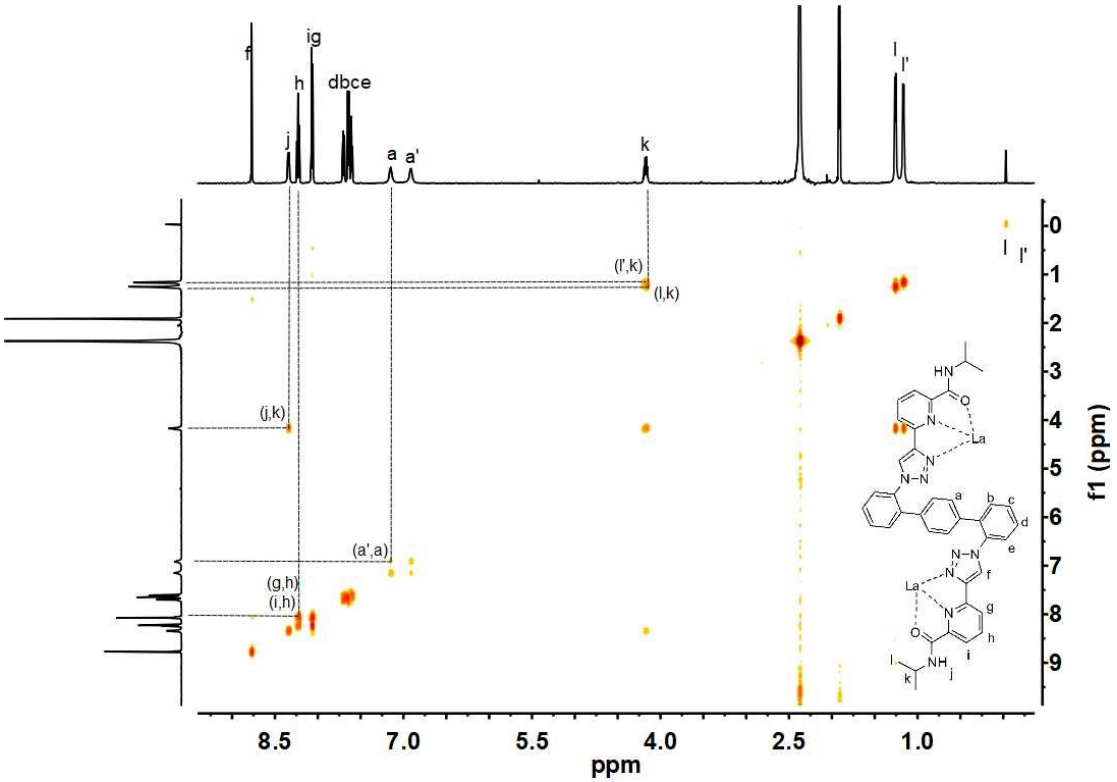

Fig. S6 ^{1}H-^{1}H COSY NMR spectrum of $(La_2\mathbf{L}_2)_n$ (600 MHz, CD_3CN, 298 K).

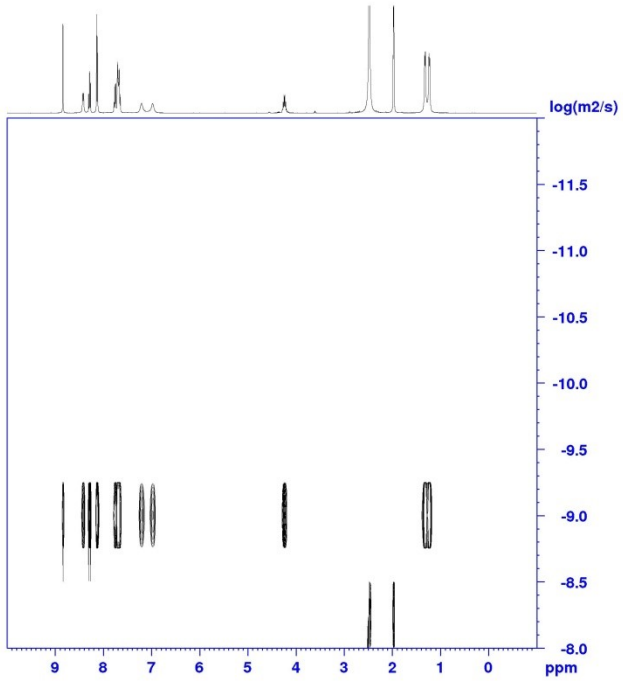

Fig. S7 ^{1}H DOSY spectrum of $(La_2\mathbf{L}_2)_n$ (D = 10.0×10^{-10} $m^2\cdot s^{-1}$, r = 6.36 Å, 400 MHz, CD_3CN, 298 K).

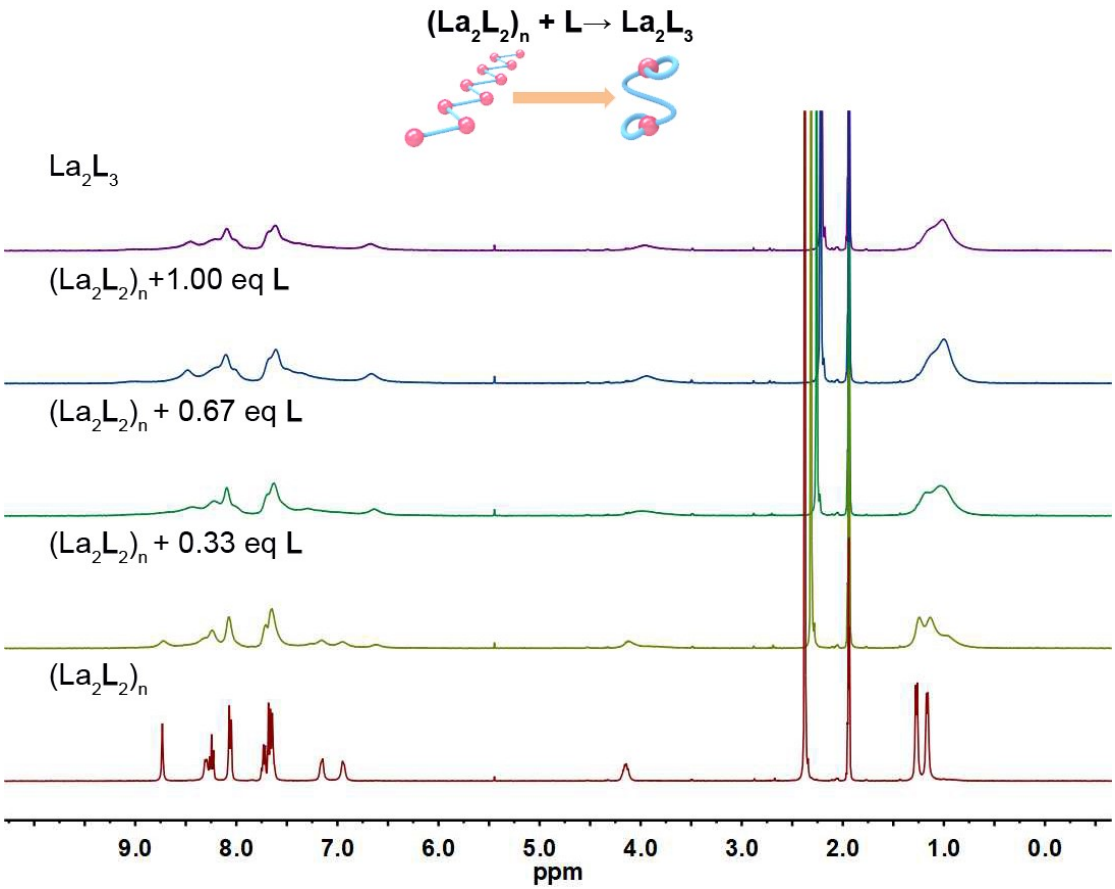

Fig. S8 ^{1}H NMR spectra of titrating $(La_2\mathbf{L}_2)_n$ with different equivalents of **L** (relative to the amount of $La_2\mathbf{L}_2$, 400MHz, CD_3CN, 298K).

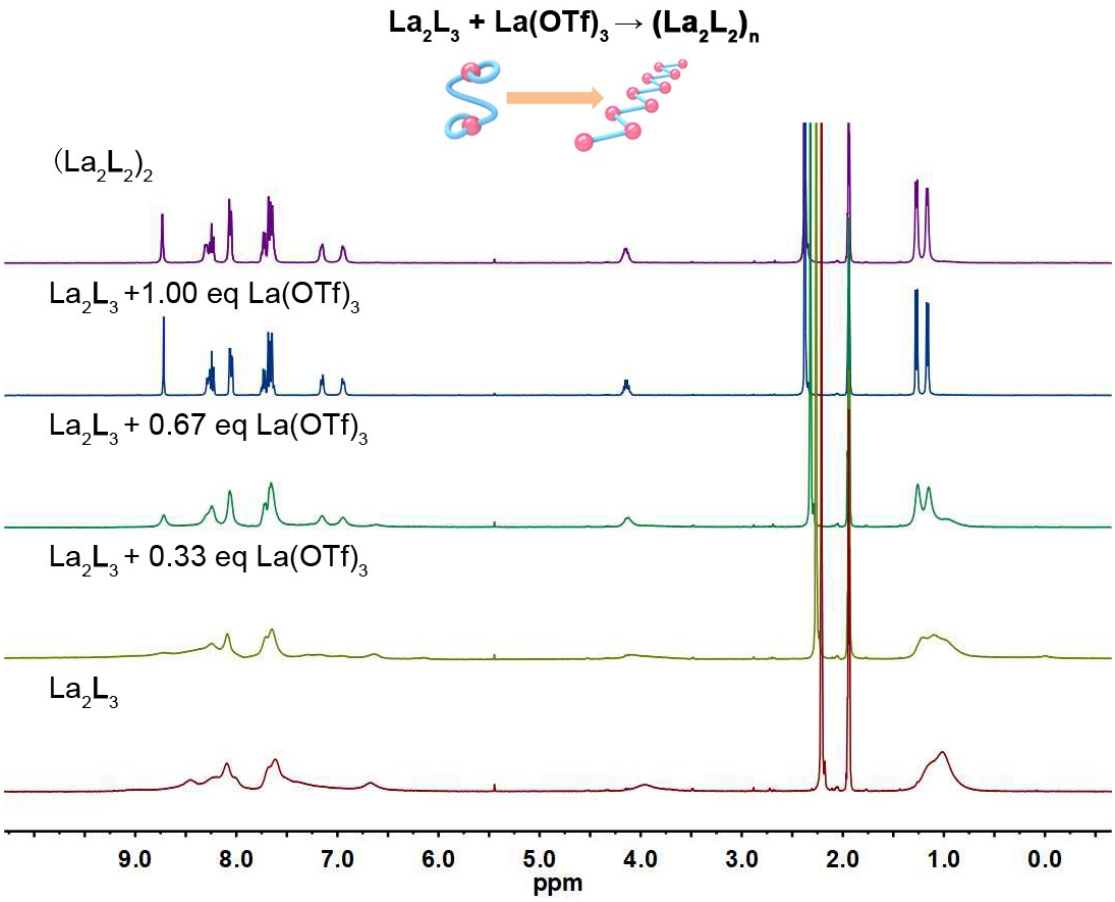

Fig. S9 ^{1}H NMR spectra of titrating $La_2\mathbf{L}_3$ with different equivalents of $La(OTf)_3$ (relative to the amount of $La_2\mathbf{L}_3$, 400MHz, CD_3CN, 298K).

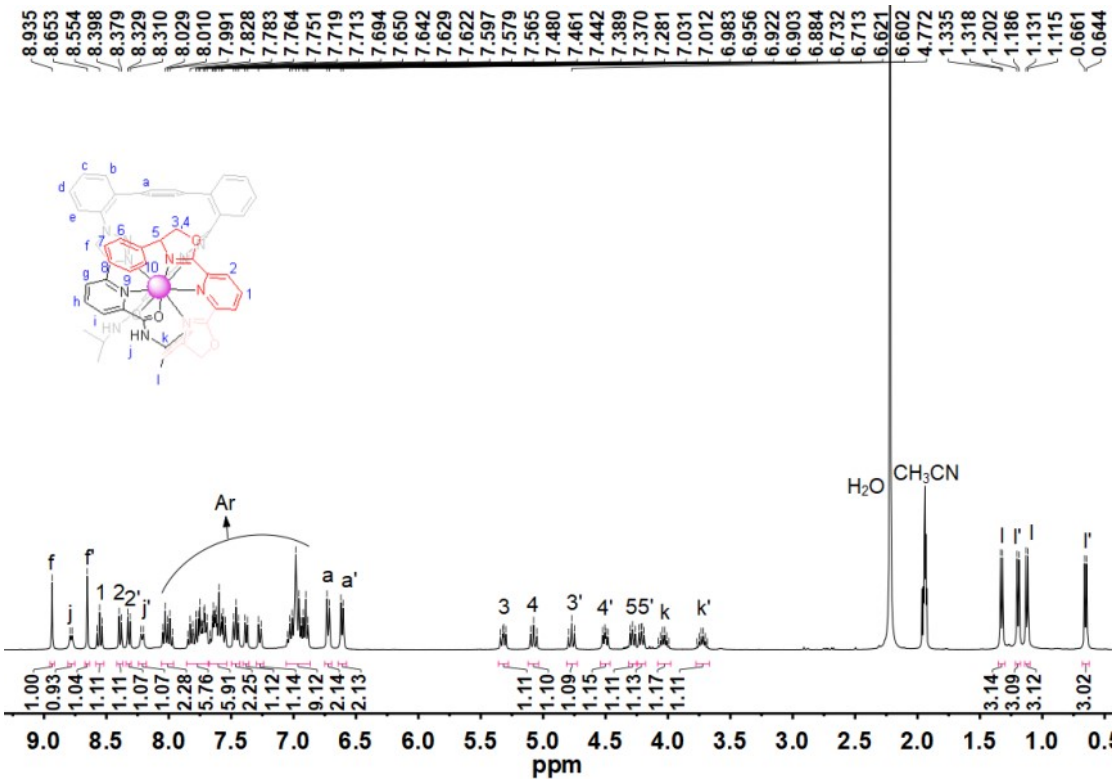

Fig. S10 ^{1}H NMR spectrum of *Δ*-La**LG**^{R} (400MHz, CD_3CN, 298K).

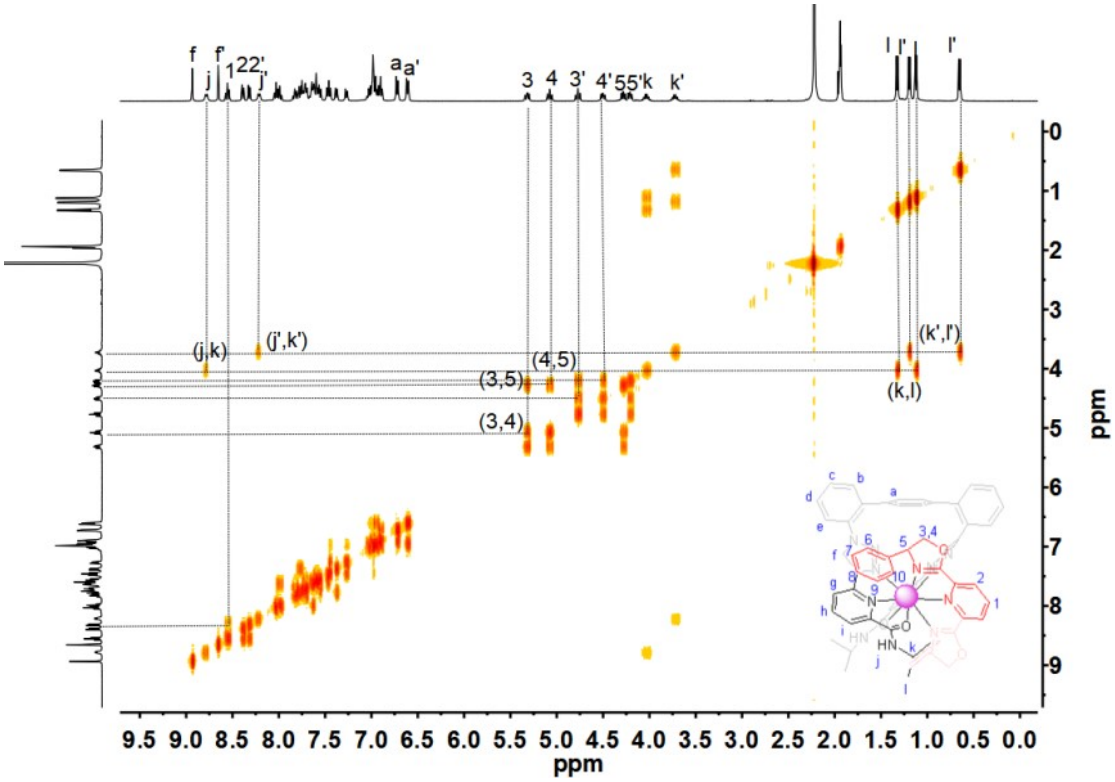

Fig. S11 ^{1}H-^{1}H COSY NMR spectrum of *Δ*-La**LG**^{R} (400 MHz, CD_3CN, 298 K).

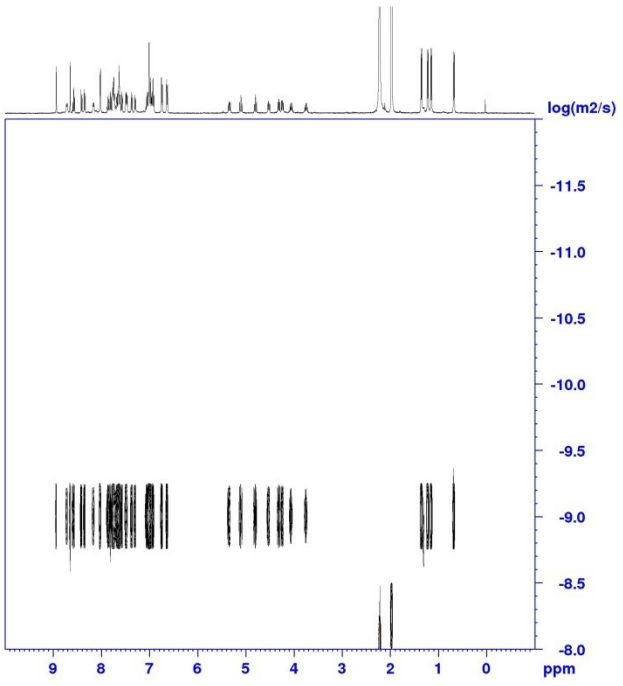

Fig. S12 ^{1}H DOSY spectrum of *Δ*-La**LG**^{R} (D=9.84×10^{-10} m^{2}s^{-1}, r = 6.46 Å, 400 MHz, CD_3CN, 298 K).

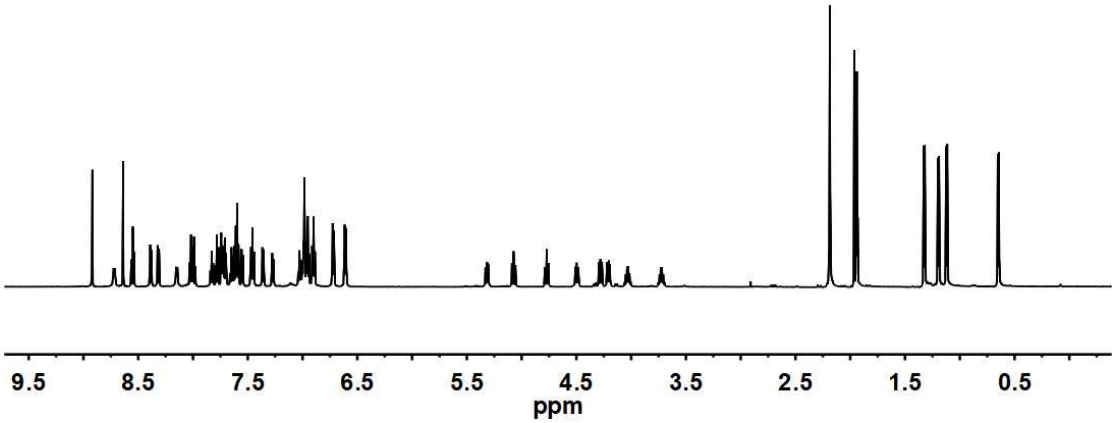

Fig. S13 ^{1}H NMR spectrum of *Λ*-La**LG**^{S} (400MHz, CD_3CN, 298K).

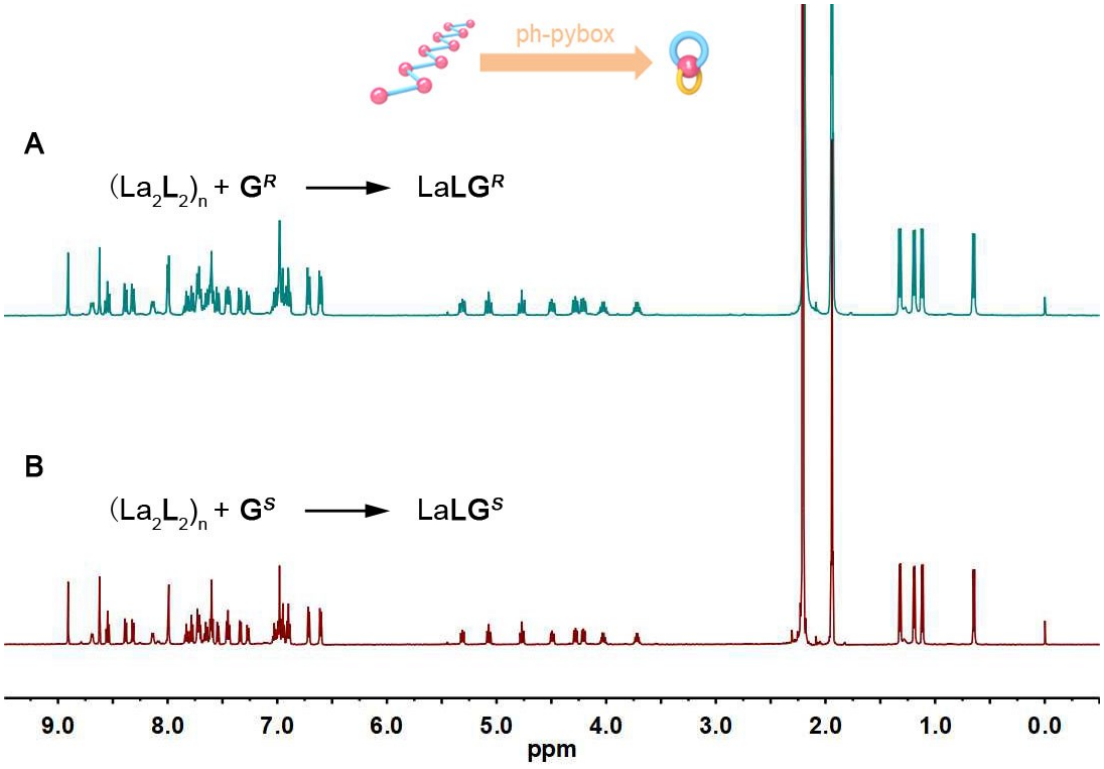

Fig. S14 ^{1}H NMR spectra of A) *Λ*-La**LG**^{R} and B) *Λ*-La**LG**^{S} transformed from $(La_2\mathbf{L}_2)_n$ by adding **G**^{R} and **G**^{S}, respectively (400MHz, CD_3CN, 298K).

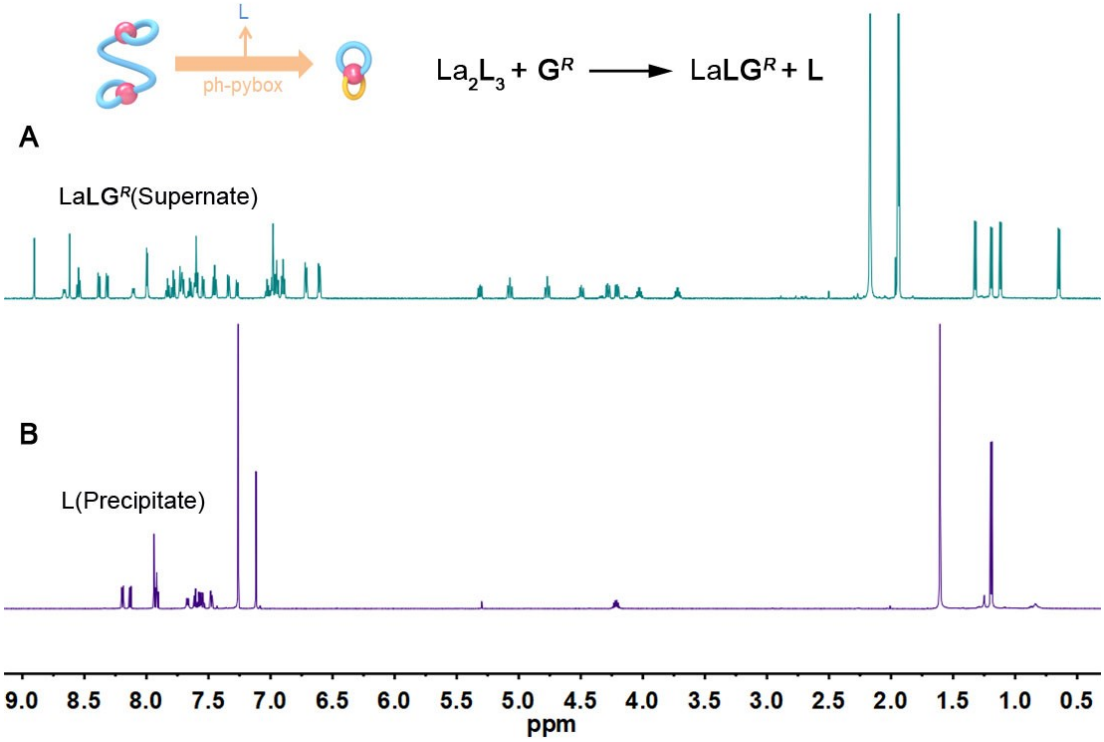

Fig. S15 ^{1}H NMR spectra of A) the supernate *Δ*-La**L**$\mathbf{G}^{R}$ (CD_3CN) and B) the precipitate **L** ($CDCl_3$) after adding 2eq $\mathbf{G}^{R}$ into $La_2\mathbf{L}_3$ (400MHz, 298K).

4. ESI-TOF-MS analyses

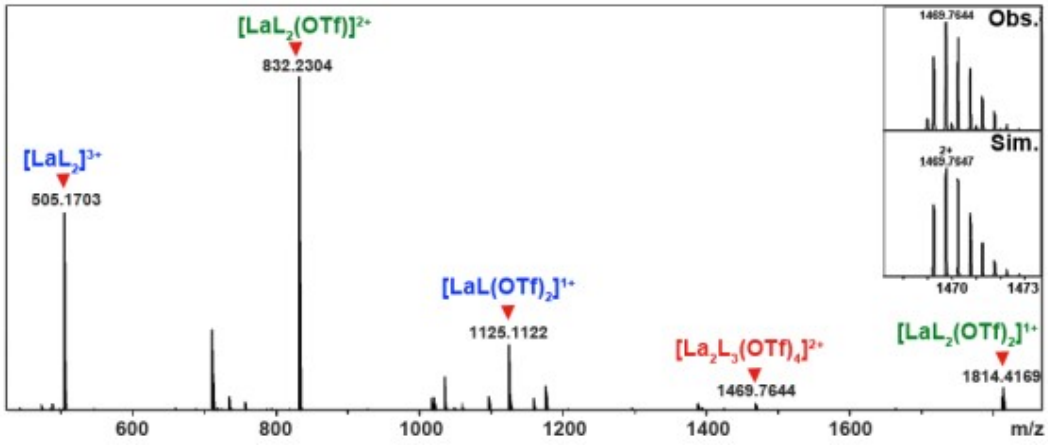

Fig. S16 ESI-TOF-MS spectra of $La_2\mathbf{L}_3$, with inserts showing the observed and simulated isotopic patterns of the peaks corresponding to $[(La_2\mathbf{L}_3)(OTf)_4]^{2+}$.

The tandem mass spectrometry (MS/MS) experiments were carried out to confirm whether La_2L_3 decomposed in the gas-phase during MS measurement. The $[(La_2\mathbf{L}_3)(OTf)_4]^{2+}$ ion (corresponding to m/z value of 1469.7644) was isolated and subjected to collisional activation with N_2 at collision energies ranging from 0 to 12 eV. Two new peaks at 1125.1122 and 1813.4160, corresponding to $[(La\mathbf{L})(OTf)_2]^{+}$

and $[(LaL_2)(OTf)_2]^+$, respectively, were detected expressly even no collision energy exerted. Along with the collision energy gradually increased to 12 eV, the chosen $[(La_2L_3)(OTf)_4]^{2+}$ ion was nearly completely dissociated into $[(LaL)(OTf)_2]^+$ and $[(LaL_2)(OTf)_2]^+$. Hence, we attributed the two species of LaL_2 and LaL to the decomposition of the dinuclear complex La_2L_3 in the gas-phase during MS measurement.

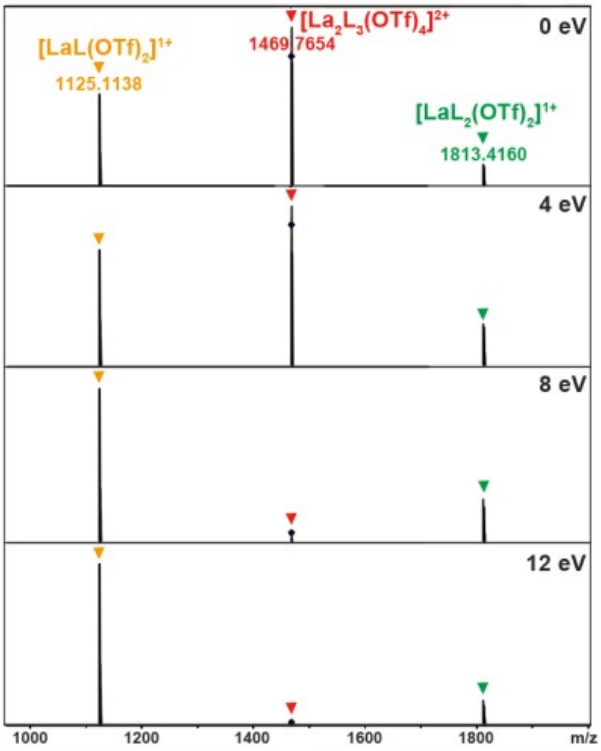

Fig. S17 Gradient tandem mass spectrometry (MS/MS) of $[(La_2L_3)(OTf)_4]^{2+}$ (m/z = 1469.7644) with various collision energies (from 0 V until 12 V). Fragment peaks were assigned to the $[(LaL)(OTf)_2]^+$ and $[(LaL_2)(OTf)_2]^+$.

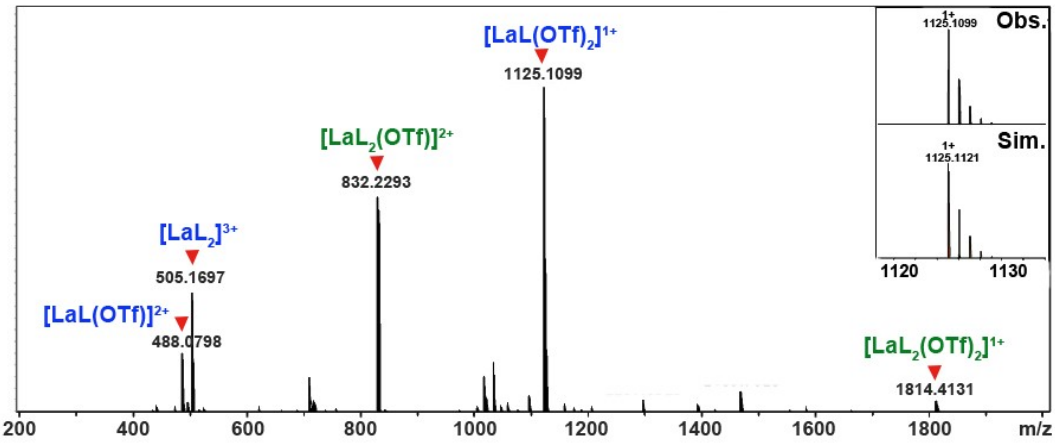

Fig. S18 ESI-TOF-MS spectra of $(La_2L_2)_n$, with inserts showing the observed and simulated isotopic patterns of the peaks corresponding to $[LaL(OTf)_2]^+$.

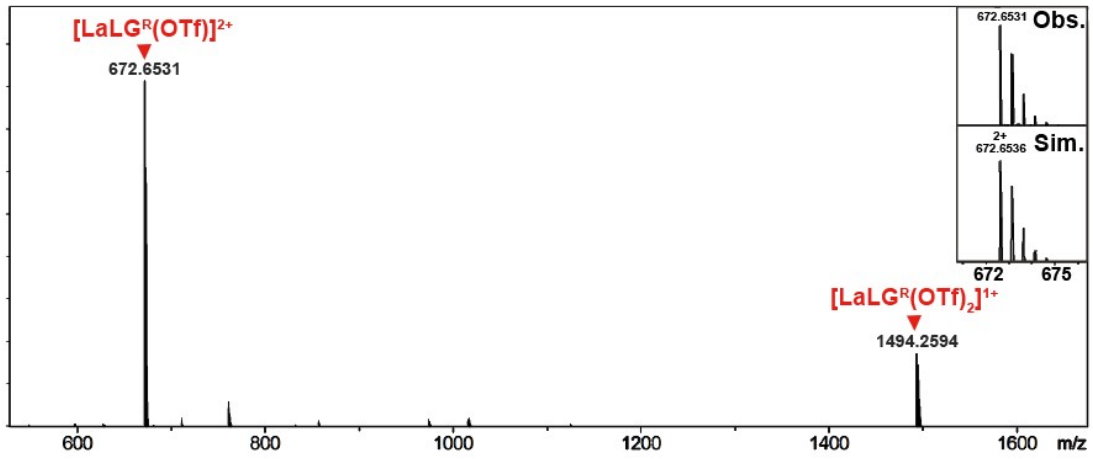

Fig. S19 ESI-TOF-MS spectra of *Δ*-La**LG**^{R}, with inserts showing the observed and simulated isotopic patterns of the peaks corresponding to [(La**LG**^{R})(OTf)]$^{2+}$.

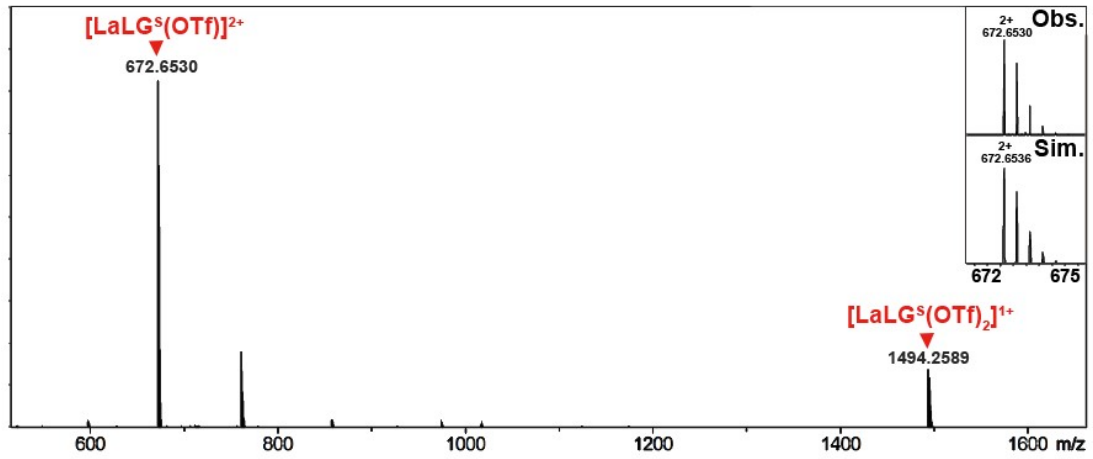

Fig. S20 ESI-TOF-MS spectra of *Λ*-La**LG**^{S}, with inserts showing the observed and simulated isotopic patterns of the peaks corresponding to [(La**LG**^{S})(OTf)]$^{2+}$.

5. X-ray single crystal diffraction analyses

Suitable single crystals for complexes $La_2\mathbf{L}_3$ and $(La_2\mathbf{L}_2)_n$ were obtained by slow diffusion of poor solvent vapor chloroform into the CH_3CN solution of complexes in several days, respectively. The X-ray diffraction studies were carried out on Bruker D8 VENTURE photon II diffractometer with Iμs 3.0 microfocus X-ray source using APEX III program. Data reduction was performed with the saint and SADABS package. All the structures were solved by direct methods and refined by full matrix least-squares on *F2* with anisotropic displacement using the SHELXTL software package[3]. Solvent molecules were highly disordered and could not be reasonably located. These residual intensities were removed by PLATON/SQUEEZE routine.[4, 5].

Crystal data for $La_2\mathbf{L}_3(ClO_4)_6$ (CCDC-2213030): Space group *P*-1, a = 14.295(3) Å, b = 23.172 (5) Å, c = 24.978(5) Å, α = 92.02(3)°, β = 98.22(3)°, γ = 96.26 (3)°, V

= 8129(3) Å^3, Z = 2, T = 100(2) K. Anisotropic least-squares refinement for the framework atoms and isotropic refinement for the other atoms on 34374 independent merged reflections (*Rint*= 0.1067) converged at residual *wR2* = 0.4313 for all data; residual *R1* = 0.1515 for 18008 observed data [$I > 2\sigma(I)$], and goodness of fit (GOF) = 1.337.

Crystal data for $[La_2\mathbf{L}_2(OTf)_6]_n$ (CCDC-2213035): Space group *P*-1, a = 12.7462(13) Å, b = 15.4664(16) Å, c = 16.5928(18) Å, α = 63.002(3)°, β = 80.962(3)°, γ = 70.020(3)°, V = 2739.2(5) Å^3, Z = 2, T = 100(2) K. Anisotropic least-squares refinement for the framework atoms and isotropic refinement for the other atoms on 10787 independent merged reflections (*Rint*= 0.4715) converged at residual *wR2* = 0.1955 for all data; residual *R1* = 0.0678 for 6841 observed data [$I > 2\sigma(I)$], and goodness of fit (GOF) = 1.041.

Table S1. Crystal data and structure refinement for complex $La_2\mathbf{L}_3$.

Identification code	$La_2\mathbf{L}_3$	
Empirical formula	C123 H111 Cl15 La2 N30 O30[+ solvent]	
Formula weight	3298.99	
Temperature	100(2) K	
Wavelength	0.71073 Å	
Crystal system	Triclinic	
Space group	P-1	
Unit cell dimensions	a = 14.295(3) Å	α= 92.02(3)°.
	b = 23.172(5) Å	β= 98.22(3)°.
	c = 24.978(5) Å	γ = 96.26(3)°.
Volume	8129(3) $Å^3$	
Z	2	
Density (calculated)	1.348 Mg/m^3	
Absorption coefficient	0.837 mm^{-1}	
F(000)	3336	
Crystal size	0.05 x 0.05 x 0.02 mm^3	
Theta range for data collection	1.241 to 26.733°.	
Index ranges	-17<=h<=18, -26<=k<=29, -31<=l<=31	
Reflections collected	113162	
Independent reflections	34374 [R(int) = 0.1067]	
Completeness to theta = 25.242°	99.9 %	
Absorption correction	None	
Refinement method	Full-matrix least-squares on F^2	
Data / restraints / parameters	34374 / 1882 / 1567	
Goodness-of-fit on F^2	1.337	
Final R indices [I>2sigma(I)]	R1 = 0.1515, wR2 = 0.3894	
R indices (all data)	R1 = 0.2174, wR2 = 0.4313	
Extinction coefficient	n/a	
Largest diff. peak and hole	4.159 and -1.165 $e.Å^{-3}$	

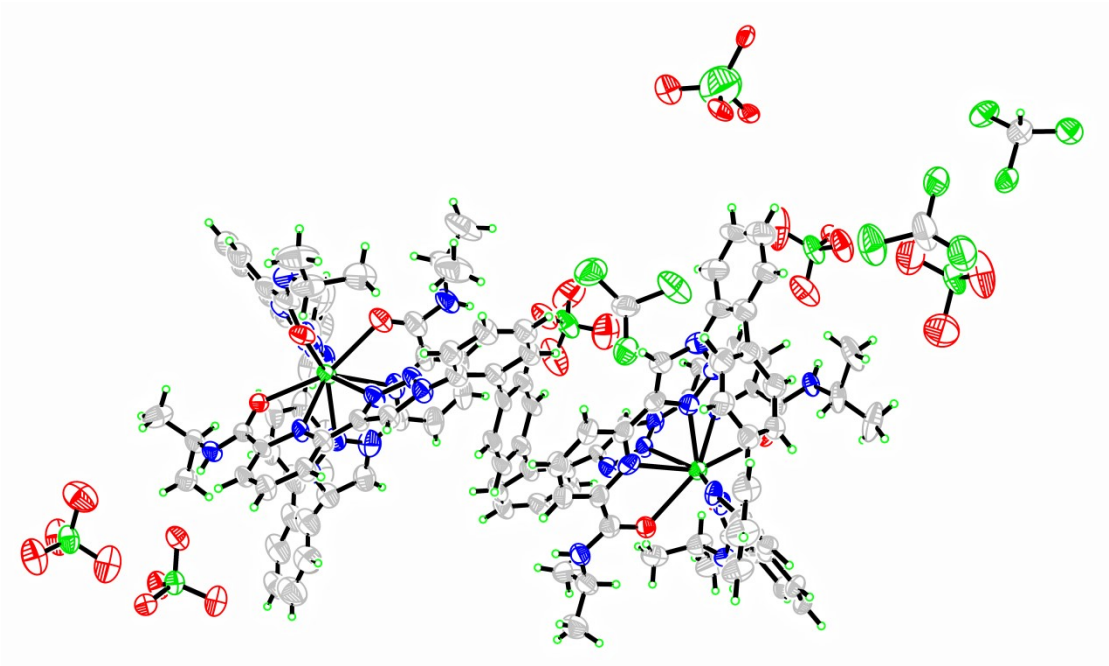

Fig. S21 Ortep drawing of the asymmetry unit in the crystal structure of $La_2\mathbf{L}_3$.

Table S2. Crystal data and structure refinement for $(La_2\mathbf{L}_2)_n$.

Identification code	$(La_2\mathbf{L}_2)_n$	
Empirical formula	C44 H37 Cl3 F9 La N10 O11 S3	
Formula weight	1394.28	
Temperature	100(2) K	
Wavelength	0.71073 Å	
Crystal system	Triclinic	
Space group	P-1	
Unit cell dimensions	a = 12.7462(13) Å	α= 63.002(3)°.
	b = 15.4664(16) Å	β= 80.962(3)°.
	c = 16.5928(18) Å	γ = 70.020(3)°.
Volume	2739.2(5) $Å^3$	
Z	2	
Density (calculated)	1.690 Mg/m^3	
Absorption coefficient	1.137 mm^{-1}	
F(000)	1392	
Crystal size	0.2 x 0.2 x 0.1 mm^3	
Theta range for data collection	2.481 to 26.032°.	
Index ranges	-15<=h<=15, -19<=k<=19, -20<=l<=20	
Reflections collected	96755	
Independent reflections	10787 [R(int) = 0.4715]	
Completeness to theta = 25.242°	99.9 %	
Absorption correction	None	
Refinement method	Full-matrix least-squares on F^2	
Data / restraints / parameters	10787 / 3 / 734	
Goodness-of-fit on F^2	1.041	
Final R indices [I>2sigma(I)]	R1 = 0.0678, wR2 = 0.1742	
R indices (all data)	R1 = 0.1128, wR2 = 0.1955	
Extinction coefficient	n/a	
Largest diff. peak and hole	1.866 and -1.501 $e.Å^{-3}$	

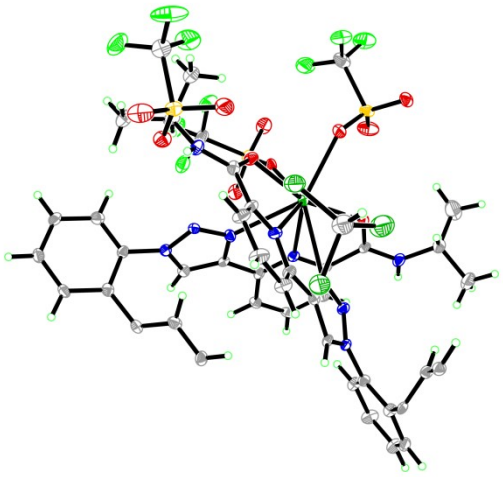

Fig. S22 Ortep drawing of the asymmetry unit in the crystal structure of $(La_2\mathbf{L}_2)_n$.

6. Molecular modeling and calculations

Molecular modeling and calculations were performed to gain further insight into the preferential formation of mono-bridged dinuclear complex ($La_2\mathbf{L_3}$).

Molecular mechanical simulations were also carried out in Materials studio 8.0. The initial conformations were adopted from the crystal structures of this mono-bridged dinuclear $La_2\mathbf{L}_3$ and previous *ΛΛ*-$La_2\mathbf{L}^{\boldsymbol{R}}_3$. The energy calculation was performed with universal forcefield. Electrostatic interaction and van der Waals interactions were calculated using atom based summation method (Table S3). The mono-bridged dinuclear structure reveals a total energy of 1280.05 kcal/mol, much lower than the helicate and mesocate isomers. These energy differences ensure that the mono-bridged dinuclear assembly is energetically more favored structure.

Table S3. Computational studies of the dinuclear complexes of $La_2\mathbf{L_3}$ with Materials Studio 8.0.

	Helicate	**Mesocate**	**Mono-bridged dinuclear**
Total energy (kcal/mol)	1448.839857	1381.062440	1280.054542
Valence energy (diag. terms) (kcal/mol)	1353.817	1270.052	1162.398
Bond(kcal/mol)	27.302	38.220	38.853
Angle(kcal/mol)	1226.138	1138.923	977.174
Torsion(kcal/mol)	99.090	89.848	139.433
Inversion(kcal/mol)	1.286	3.062	6.937
Non-bond energy (kcal/mol)	95.023	111.011	117.657
van der Waals(kcal/mol)	95.023	111.011	117.657
Electrostatic(kcal/mol)	0.000	0.000	0.000

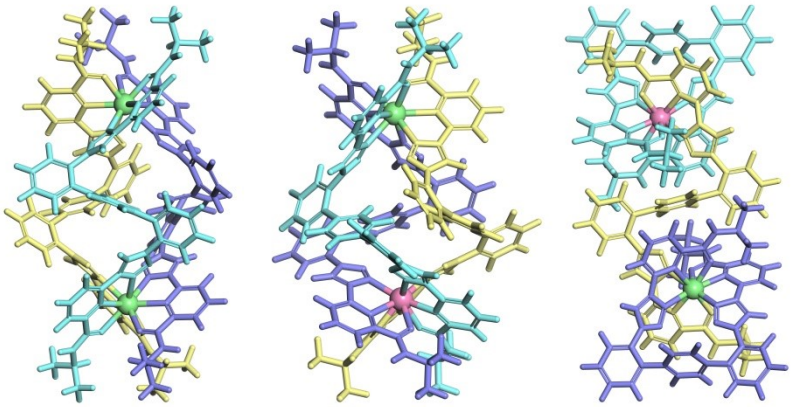

Figure S23 The MM modelled structures for the isomers of La_2L_3 with their total energies. For clarity, the ligands were coloured differently.

7. Supporting references

1. X. Q. Guo, L. P. Zhou, L. X. Cai and Q. F. Sun, *Chemistry – A European Journal*, 2018, **24**, 6936-6940.
2. R. Chen, Q.-Q. Yan, S.-J. Hu, X.-Q. Guo, L.-X. Cai, D.-N. Yan, L.-P. Zhou and Q.-F. Sun, *Org. Chem. Front.*, 2021, **8**, 2576-2582.
3. G. M. Sheldrick, *Acta Crystallogr. Sect. A*, 2008, **64**, 112-122.
4. A. L. Spek, *J. Appl. Crystallogr.*, 2003, **36**, 7-13.
5. A. L. Spek, *Acta Crystallogr. Sect. C-Struct. Chem.*, 2015, **71**, 9-18.